Physical properties and electronic structure of the two-gap superconductor V_2Ga_5

P.-Y. Cheng,[1,2,3] Mohamed Oudah,[4] T.-L. Hung,[5] C.-E. Hsu,[6] C.-C. Chang,[1,2,3,7] J.-Y. Haung,[8] T.-C. Liu,[8] C.-M. Cheng,[7,9,10,3] M.-N. Ou,[5] W.-T. Chen,[11,12,3] L. Z. Deng,[13] C.-C. Lee,[6] Y.-Y. Chen,[5] C.-N. Kuo,[1,3] C.-S. Lue,[1,3] Janna Machts,[14,15] Kenji M. Kojima,[4,14] Alannah M. Hallas,[4,16,17] and C.-L. Huang[1,2,3,*]

[1]*Department of Physics, National Cheng Kung University, Tainan 701, Taiwan*
[2]*Center for Quantum Frontiers of Research & Technology (QFort), National Cheng Kung University, Tainan 701, Taiwan*
[3]*Taiwan Consortium of Emergent Crystalline Materials, National Science and Technology Council, Taipei 10622, Taiwan*
[4]*Stewart Blusson Quantum Matter Institute, University of British Columbia, Vancouver, BC, V6T 1Z4, Canada*
[5]*Institute of Physics, Academia Sinica, 128 Sec. 2, Academia Rd., Nankang, Taipei 11529, Taiwan*
[6]*Department of Physics, Tamkang University, New Taipei 251301, Taiwan*
[7]*National Synchrotron Radiation Research Center (NSRRC), Hsinchu 30076, Taiwan*
[8]*Department of Physics, National Tsing Hua University, Hsinchu 30013, Taiwan*
[9]*Department of Physics, National Sun Yat-sen University, Kaohsiung 80424, Taiwan*
[10]*Department of Electrophysics, National Yang Ming Chiao Tung University, Hsinchu 300 Taiwan*
[11]*Center for Condensed Matter Sciences, National Taiwan University, Taipei 10617, Taiwan*
[12]*Center of Atomic Initiative for New Materials, National Taiwan University, Taipei 10617, Taiwan*
[13]*Texas Center for Superconductivity and Department of Physics, University of Houston, Houston, Texas 77204, USA*
[14]*TRIUMF Centre for Molecular and Material Science (TRIUMF-CMMS), University of British Columbia, Vancouver, BC, V6T 2A3, Canada*
[15]*School of Physics and Astronomy, University of Edinburgh, Edinburgh EH9 3FD, United Kingdom*
[16]*Department of Physics & Astronomy, University of British Columbia, Vancouver, BC, V6T 1Z1, Canada*
[17]*Canadian Institute for Advanced Research, Toronto, ON, M5G1M1, Canada*

(Received 21 April 2024; accepted 18 June 2024; published 4 September 2024)

We present a thorough investigation of the physical properties and superconductivity of the binary intermetallic V_2Ga_5. Electrical resistivity and specific heat measurements show that V_2Ga_5 enters its superconducting state below $T_{sc} = 3.5$ K, with a critical field of $H_{c2,\perp c}(H_{c2,||c}) = 6.5(4.1)$ kOe. With $H \perp c$, the peak effect was observed in resistivity measurements, indicating the ultrahigh quality of the single crystal studied. The resistivity measurements under high pressure reveal that the T_{sc} is suppressed linearly with pressure and reaches absolute zero around 20 GPa. Specific heat and muon spin relaxation measurements indicate that the two-gap *s*-wave model best describes the superconductivity of V_2Ga_5. The bands near the Fermi level around the Z and Γ points are observed and analyzed by the angle-resolved photoemission spectroscopy measurements and first-principles band structure calculations. We therefore conclude that V_2Ga_5 is a phonon-mediated two-gap *s*-wave superconductor.

DOI: 10.1103/PhysRevResearch.6.033253

I. INTRODUCTION

Intermetallic compounds composed of metals of *d*- and *p*-shell electrons have been one of the most studied series in condensed matter physics owing to their abundance and their chemical and physical properties. In particular, due to the low-melting points of metals with *p*-shell electrons, high-quality single crystals can often be grown by the common flux method and hence detailed property measurements can be conducted [1,2].

Among mentioned intermetallic compounds, the V-Ga binary system has gained extra interest because some compounds in this family are superconductors. The superconductor V_3Ga is best known for its relatively high transition temperature ($T_{sc} = 15$ K), high critical currents, and fields [3,4]. In contrast, for another superconductor V_2Ga_5, relevant research reports are quite scarce. The electrical resistivity, magnetic susceptibility, and specific heat measurements conducted down to 1.8 K have been reported, which showed V_2Ga_5 enters the superconducting state below $T_{sc} = 3.5$ K and its critical field is about 4–5 kOe [5–7]. Very recently, Xu *et al.* report multigap superconductivity in V_2Ga_5 via specific heat and thermal conductivity measurements [8]. To verify this result and acquire a deeper understanding of the superconductivity and the physical properties of V_2Ga_5, it is essential to expand the specific heat measurements to lower temperatures and conduct a comprehensive study using various experimental techniques. We carried out electrical resistivity measurements with magnetic fields applied parallel and perpendicular to the crystallographic *c* axis and constructed the critical field versus T_{sc} phase diagrams.

*Contact author: clh@phys.ncku.edu.tw

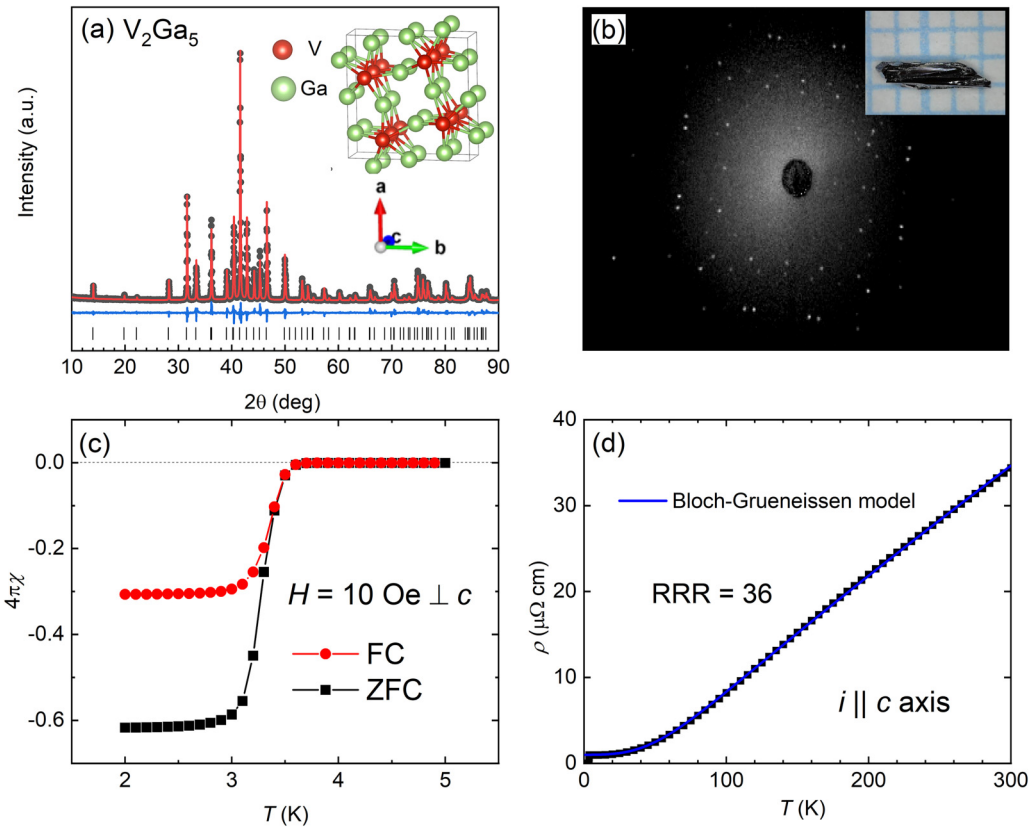

FIG. 1. (a) Observed (circle), calculated (red line), and differences (blue line) x-ray powder-diffraction patterns of V_2Ga_5 at room temperature. Bragg reflections for V_2Ga_5 of the space group $P4/mbm$ are labeled as vertical bars. The inset shows the crystal structure of one unit cell. Note that a and b are equivalent in tetragonal symmetry. (b) Laue x-ray pattern taken along the tetragonal [001] direction. The inset shows a photo of the crystal. (c) Field-cooled (FC) and zero-field-cooled (ZFC) magnetic susceptibility measurements at $H = 10$ Oe applied perpendicular to the c axis. (d) Zero-field temperature dependence of electrical resistivity with a fit by the Bloch-Grueneissen model.

Under high pressure, T_{sc} is suppressed linearly to absolute zero around $P = 20$ GPa. This result is in line with the phonon mediated superconductivity in V_2Ga_5. A consistent conclusion about the two-gap s-wave order parameter is drawn from two complementary experiments: specific heat as a bulk probe and muon spin relaxation as a local probe. This conclusion was further validated by angle-resolved photoemission spectroscopy experiments and first-principles calculations.

II. RESEARCH METHODS

V_2Ga_5 single crystals were prepared by a flux method using excess Ga [6,7]. High-purity V powder and Ga pieces were weighed according to the composition V_6Ga_{94} and placed in an alumina crucible, which was then sealed in an evacuated quartz tube. Higher vanadium concentrations were also tested but yielded needle-shape samples, as been reported in Ref. [5–7]. The quartz tube was heated to 1000 °C at a rate of 100 °C/h, held at this temperature for 48 h and then cooled to 550 °C at a rate of 2.5 °C/h. Excess Ga flux was spun off using a centrifuge. The remaining Ga droplets on the surface were removed by etching in diluted HCl. As shown in the inset of Fig. 1(b), the obtained single crystals have rodlike shape along the c axis with typical dimensions $\sim 2 \times 2 \times 8$ mm^3. Pulverized V_2Ga_5 was characterized by x-ray powder diffraction with Cu-Kα radiation (Bruker D2 Phaser diffractometor) at room temperature. The crystal structure was analyzed using DIFFRAC.TOPAS program [9] with the Rietveld refinement method. Single crystal x-ray diffraction data were collected with a Rigaku Synergy-S diffractometer with Mo-K radiation at 300 and 100 K. Images of representative reciprocal planes are shown in Ref. [10]. The orientation of crystal was confirmed by a Laue x-ray diffraction method. Reciprocal planes from single crystal x-ray diffraction and Laue diffractograms validate the good quality of the single-crystalline samples and an example is shown in Fig. 1(b).

Magnetic susceptibility was measured using a Quantum Design (QD) magnetic property measurement system. Ambient-pressure resistivity and specific heat were measured using a QD Dynacool physical properties measurement system (PPMS) equipped. For high-pressure resistivity measurements, we used a diamond anvil cell (DAC) placed in a ^{3}He cryostat. We used hexagonal boron nitride powder as the pressure medium and hence the pressure is nonhydrostatic.

Muon spin relaxation (μSR) measurements were performed on the M15 beam line at TRIUMF using the Pandora dilution refrigerator spectrometer. Several dozen needlelike crystals of V_2Ga_5 were co-aligned by eye on a silver sample plate using GE varnish. Measurements were performed over a temperature range of 0.025 to 6 K in both zero field and in an applied transverse field of 300 Oe. To achieve an accurate zero field, reference measurements were performed on silicon,

which through the formation of muonium atoms with a two orders of magnitude larger gyromagnetic ratio than the muon, allows the magnetic field to be zeroed to within 10^{-2} Oe [11]. In the zero field measurements, the muons were implanted with their spins parallel to the *ab* plane of V_2Ga_5 while in the transverse field measurements, the muons are implanted with their spins along the *c* axis and the transverse field is applied parallel to the *ab* plane. The collected data were analyzed with MUSRFIT [12].

Angle-resolved photoemission spectroscopy (ARPES) experiment was conducted at beamline BL21B1 of the Taiwan Light Source, affiliated with the National Synchrotron Radiation Research Center. The whole experiment data were collected by Scienta R4000 analyzer within ultrahigh vacuum (UHV) condition, utilizing an angular resolution calibrated to 0.5°. The sample was cleaved in the preparation chamber maintained under UHV conditions to ensure the freshness of the crystal plane, with a pressure of approximately 8.9×10^{-11} torr. The in situ cleavage plane is either the *a*-*c* or *b*-*c* plane. The spectra were obtained at 89 K, using photon energies between 52 and 86 eV, with the measurements achieving an overall energy resolution exceeding 22 meV.

The first-principles calculations were performed using QUANTUM ESPRESSO [13] code with PBE exchange-correlation functional. The atomic positions were optimized at the experimental lattice constants. The plane wave cutoff was set to 100 Ry and the k points were sampled on a $4 \times 4 \times 12$ grid. The electronic structure was calculated with the inclusion of spin-orbit coupling. For the electron-phonon properties, the EPW [14] software was used to interpolate the electron-phonon coupling matrix elements from the coarse grid ($4 \times 4 \times 12$ *k* and $2 \times 2 \times 6$ *q* grids) to the finer grid ($20 \times 20 \times 60$ *k* and $10 \times 10 \times 30$ *q* grids). For the computational efficiency, the effect of spin-orbit coupling has been neglected when calculating the electron-phonon-related properties using the linear response framework. Note that the band structure obtained here without adopting any Hubbard correction is similar to the GGA + *U* result with $U = 1$ eV, where the band topology at the Fermi level is consistent with the result of $U = 3.5$ eV [8].

III. RESULTS AND DISCUSSIONS

A. Crystal structure

The refined structural parameters are summarized in Table I. It was shown that the crystal is single phase and crystallized in tetragonal space group $P4/mbm$ (No. 127), which is in consistent with reported crystal structure [15]. The crystal structure can be viewed as connecting and piling of slightly distorted vanadium-centered VGa_{10} pentagonal pillars, in which consisting of eight longer V-Ga1 bonds of 2.72 Å and two shorter V-Ga2 bonds of 2.59 Å.

B. Electrical resistivity

As V_2Ga_5 enters the superconducting state below $T \sim 3.5$ K, a diamagnetic signal is clearly seen in magnetization measurements, as shown in Fig. 1(c). The demagnetization effect has been taken into account [16]. However, due to the sample's needlelike shape and irregular cross-section, it is difficult to correctly estimate the demagnetization factor. This

TABLE I. Crystal data and structural refinement for V_2Ga_5. *a* and *c* are lattice parameters. *V* is the unit-cell volume. B_{iso} is the thermal parameter. χ^2 represents the goodness of fit. R_{wp} and R_p are weighted and unweighted profile *R* factors, respectively, obtained from the refinement results. The gallium atom occupies Wyckoff positions Ga1 2*d* (1/2, 0, 0) and Ga2 8*i* (*x*, *y*, 0), while vanadium atom occupies V 4*h* (x, $x + 1/2$, 1/2) position.

Tetragonal $P4/mbm$ (No. 127)						
$a = 8.9716(1)$ Å, $c = 2.69272(4)$ Å, $V = 216.737(7)$ Å^3						
Atom	*x*	*y*	*z*	Occupancy	B_{iso}	Site
Ga1	0.2942(1)	0.5611(1)	0	1.000	0.02(4)	8*i*
Ga2	0.5	0	0	1.000	0.02	2*d*
V	0.3212(2)	0.8212(2)	0.5	1.000	0.09(6)	4*h*
$\chi^2 = 1.60$, $R_{wp} = 11.36$ % and $R_p = 8.73$ %						

results in the ZFC curves reaching $4\pi\chi \sim -0.6$, compared to -1 for a 100% superconducting volume fraction. The later specific heat data, as shown in Fig. 3, will demonstrate that the sample indeed has the full superconducting volume fraction ($C/T \to 0$ as $T \to 0$). Figure 1(d) shows the temperature dependence of electrical resistivity ρ for current along the tetragonal *c* axis under zero magnetic field. The residual resistivity $\rho_0 \sim 1.0$ $\mu\Omega$ cm (the value at the temperature right above the superconducting transition) and the residual resistivity ratio $\mathrm{RRR} = \rho_{300\,\mathrm{K}}/\rho_{4\,\mathrm{K}} = 36$ are both comparable with the previous result [7]. The normal state ρ could be described by the Bloch-Grueneisen model,

$$\rho = \rho_0 + A\left(\frac{T}{\theta_R}\right)^n \int_0^{\frac{\theta_R}{T}} \frac{x^n}{(e^x - 1)(1 - e^{-x})} dx, \qquad (1)$$

where *A* is a constant related electron-phonon interactions, θ_R is the Debye temperature as obtained from resistivity measurements, and *n* is an integer that depends upon the nature of interaction. The excellent fit results in $A = 88.0$ $\mu\Omega$ cm and $\theta_R = 369$ K. An exponent $n = 3$ can best describe the data, implying the resistance in V_2Ga_5 is mainly due to $s - d$ scattering, as is the case for transition metals [17].

Next we turn to magnetic field effect on low-*T* resistivity. Figures 2(a) and 2(b) show the data measured with the magnetic field applied perpendicular to and parallel to the *c* axis, respectively. Two different samples were used. The difference in normal state ρ values between the two field directions is mostly attributed to errors in measuring the dimensions of the samples. The superconducting transition temperature T_{sc} was determined as the temperature where two linear fits above and below the resistivity drop intersect, as shown by an arrow in Fig. 2(c). The good quality of our samples is confirmed by a sharp transition into the superconducting state at zero field. Upon application of a magnetic field, the transition broadens and moves to lower temperatures as expected. The critical field of $H_{c2,\perp c}(H_{c2,||c}) = 6.5$ (4.1) kOe is much smaller than the Pauli limited value ($H_{c2} = 1.84T_{sc} = 64$ kOe) and comparable to the value reported in the literature [8]. Interestingly, ρ shows the peak effect, which has been dubbed a rise in ρ for a certain range of magnetic fields below the onset of the superconducting transition [18],

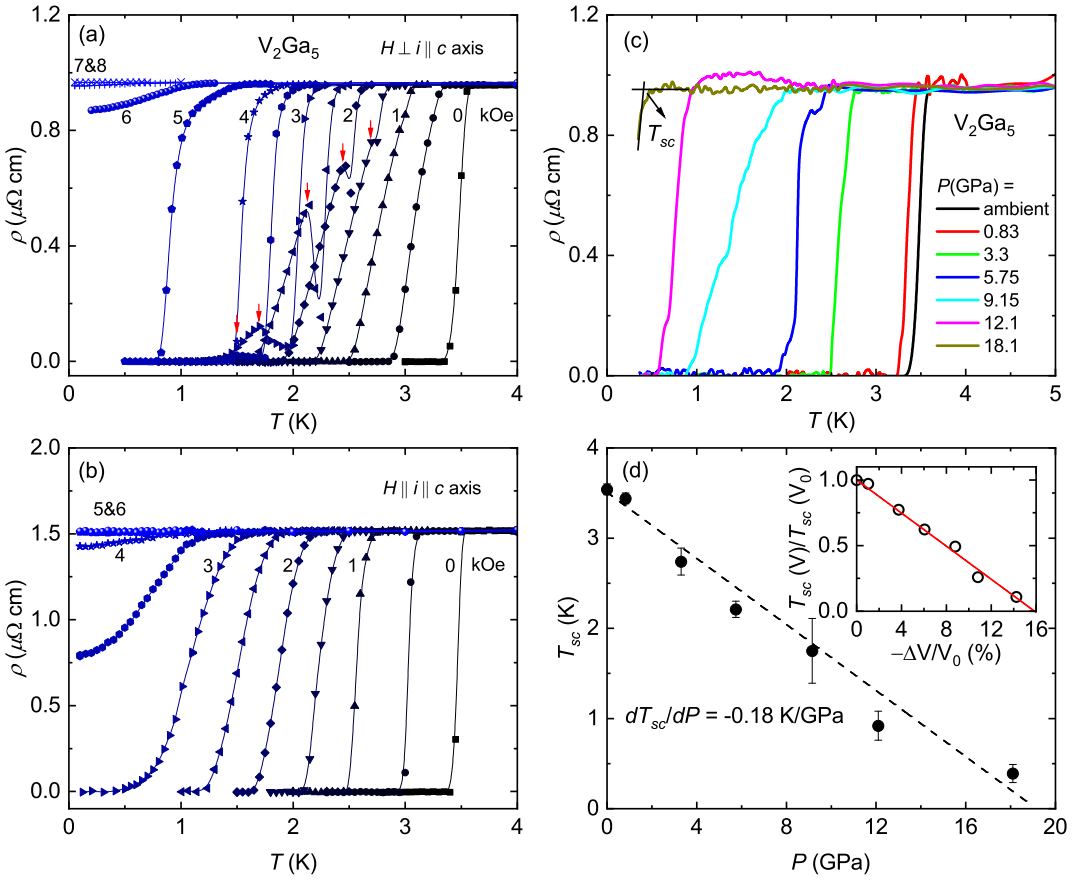

FIG. 2. Field and pressure dependence of the superconducting transition in resistivity of V_2Ga_5. (a) ρ with H applied perpendicular to the c axis for V_2Ga_5. From right to left, $H = 0$, 0.5, 1, 1.5, 2, 2.5, 3, 3.5, 4, 5, 6, 7, and 8 kOe. The downward red arrows point out the local resistivity maximum. (b) ρ with H applied parallel to the c axis. From right to left, $H = 0$, 0.5, 1, 1.5, 2, 2.5, 3, 3.5, 4, 5, and 6 kOe. Current $i = 0.1$ mA is applied along the c axis. (c) Temperature dependence of resistivity at different pressures P for V_2Ga_5. The applied current is along the c axis. An arrow demonstrates how T_{SC} was determined. (d) T_{sc} vs P. The inset shows the relative pressure shift of T_{sc} as function of the relative volume change. The dashed and solid lines are linear fits through data points.

with $H \perp c$ axis, as shown in Fig. 2(a). This sudden increase in ρ is observable for H between 1.5 and 3.5 kOe at the measured current density of $\sim$1 A/cm^2, and is reversible for increasing and decreasing the temperatures. The peak effect has been observed in several single crystal superconductors with two- or three-dimensional crystal structures [18–24]. The peak effect may be attributed to the absence of pinning centers in the sample, indicating high sample quality. This allows the vortex to flow around the sample, thereby forming a route for the current to dissipate energy [25]. We note that this is the first time the peak effect is observed in V_2Ga_5. It is absent in the data reported by Xu *et al.* where the sample has a higher residual resistivity [8]. We summarize the superconducting parameters of V_2Ga_5 derived from current work and the literature in Table II.

C. Pressure dependence of superconductivity

The pressure effect is a useful tool for varying the primary parameters that determine superconductivity, such as the density of states at the Fermi energy, the phonon frequency, and the coupling constant of electrons and phonons, without introducing chemical disorder. [26]. We investigated the pressure effect on superconductivity of V_2Ga_5 as shown in Figs. 2(c) and 2(d). Upon applying pressure, T_{sc} decreases linearly at a rate of -0.18 K/GPa up to $P = 18.1$ GPa, from which we extrapolate $T_{sc} \to 0$ around $P = 20$ GPa. We noticed a larger

TABLE II. Superconducting parameters derived from current work and the literature. ξ stands for the coherence length of superconducting Cooper pairs.

Parameters	Ref. [6]	Ref. [7]	Ref. [8]	Present work
T_{sc}	3.59	3.3	3.6	3.5
$H_{c2,\perp c}(0)$(kOe)	3-4	–	5.7	6.5
$H_{c2,\|\|c}(0)$(kOe)	–	–	4.9	4.1
$H_{c1,\perp c}(0)$(kOe)	–	–	–	0.036
$H_{c1,\|\|c}(0)$(kOe)	–	–	–	0.072
$dH_{c2,\perp c}/dT\|_{T=T_{sc}}$(kOe/K)	–	–	–	-1.85
$dH_{c2,\|\|c}/dT\|_{T=T_{sc}}$(kOe/K)	–	–	–	-1.01
ξ_{ab}/ξ_c	–	–	–	1.83
γ_n (mJ mol K^2)	–	16.7 ± 0.2	17.92	17.8 ± 0.1
β (mJ mol K^4)	–	0.448	0.024	0.20 ± 0.01
$\theta_D(K)$	–	312	–	408
$C_e/\gamma_n T_{sc}$	–	0.64	0.92	1.0
$2\Delta_1/k_B T_{sc}$	–	–	–	3.6
$2\Delta_2/k_B T_{sc}$	–	–	–	1.5

uncertainty of T_{sc} in the 9.15 GPa measurement, which is due to pressure inhomogneity across the sample in a nonhydrostatic pressure environment.

In order to convert the applied pressure to volume compression, the bulk modulus $B \equiv V \times (dP/dV)$ needs to be known. Since there are no available experimental data of $B_{V_2Ga_5}$, we estimate it using a Voigt-Reuss approximation method: from the bulk moduli of pure constituents B_i with relative concentration f_i in the compound, we calculate $B = (B_{\text{Voigt}} + B_{\text{Reuss}})/2$ with $B_{\text{Voigt}} = \sum f_i B_i$ and $1/B_{\text{Reuss}} = \sum f_i/B_i$ yielding $B_{V_2Ga_5} \sim 78.4$ GPa [17,27]. For a range of intermetallic compounds, this method yields B values in agreement of with experimental data [28]. We then used a Murnaghan equation of state:

$$B = B_0 + p\frac{dB}{dP}\bigg|_{p=0} \tag{2}$$

and for cell volume one has

$$\frac{V}{V_0} = \left[1 + \frac{\frac{dB}{dP}|_{p=0}}{B_0}p\right]^{-1/\frac{dB}{dP}|_{p=0}}, \tag{3}$$

where B_0 and V_0 are bulk modulus and cell volume at ambient pressure, respectively. For $\frac{dB}{dP}|_{p=0}$, an empirical value of 5 was used, which was found for most compounds [29]. The obtained T_{sc} as a function of relative volume change is shown in the inset of Fig. 2(d) where a linear relationship is observed. This behavior has been shown in a plethora of low temperature superconductors, which indicates phonon hardening under pressure, and hence suggest a phonon-mediated superconductivity for V_2Ga_5 [26].

D. Specific heat

Figure 3(a) shows the temperature dependence of the specific heat C/T of V_2Ga_5 under different magnetic fields $H =$ 0 to 8 kOe. In zero field, a jump in $C(T)$ representing the superconducting transition is observed at around 3.5 K, consistent with the finding in the previous specific-heat studies [7,8]. As the temperature decreases, C/T approaches zero, indicating a complete superconducting volume of the sample. Below $T \sim 0.1$ K, an upturn of C/T due to a nuclear Schottky contribution from all nuclei with nonzero nuclear moments [30]. This upturn occurs at higher temperatures with an increase of the magnetic field as expected [31]. The superconducting transition can be traced up to $H = 5$ kOe and cannot be observed at $H \geqslant 6$ kOe. Thus, the normal-state specific heat $C_n(T)$ is extracted from the $H = 8$ kOe data between $T = 1$ to 4 K to avoid the nuclear contribution at lower temperatures. $C_n(T)$ can be described as $C_n(T) = \gamma_n T + \beta T^3$, where $\gamma_n T$ is the normal electronic contribution and βT^3 represents the phonon contribution. The fit (not shown) leads to $\gamma_n = 17.82 \pm 0.10$ mJ/mol K^2 and $\beta = 0.200 \pm 0.012$ mJ/mol K^4. From β, we derive the corresponding Debye temperature $\theta_D = 408$ K, which is close to the value determined from our Bloch-Grueneissen fit to the resistivity, $\theta_R = 369$ K [Fig. 1(d)]. The obtained $\gamma_n T$ value is consistent with that in Ref. [8], but our β value is almost one order of magnitude higher. This is most probably due to the fact that Xu *et al.* introduced a higher order term ($C_n(T) = \gamma_n T + \beta T^3 + \delta T^5$) to describe the phonon contribution to the specific heat. Their fit yields an unphysically low θ_D, and we did not find a T^5 term

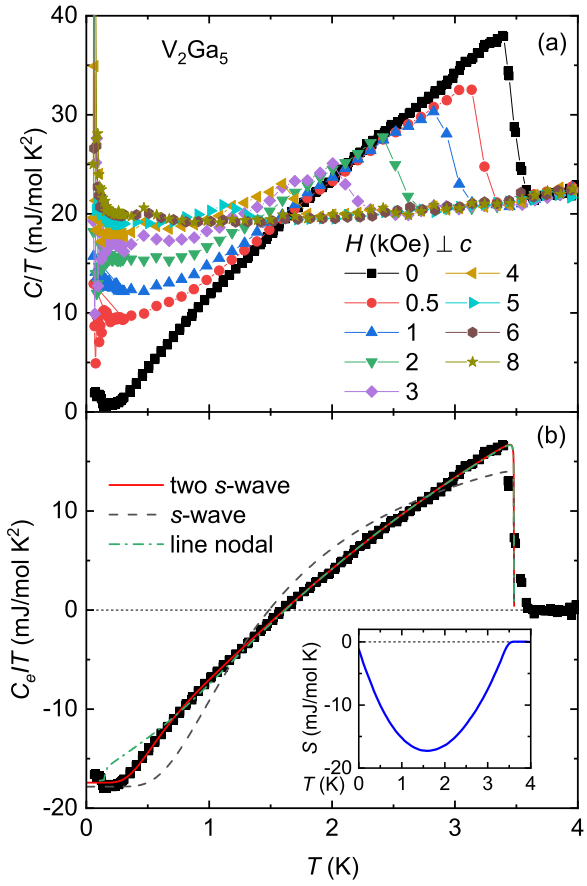

FIG. 3. (a) Temperature dependence of specific heat plotted as C/T vs T at various magnetic fields applied perpendicular to the c axis for V_2Ga_5. (b) Temperature dependence of the superconducting-transition contribution to the specific heat C_e/T. The solid, dashed, and dash-dot lines are fits using a two-gap s-wave, a single-gap s-wave, and a line node d-wave models, respectively. Inset shows that the entropy (S), calculated from the data in the main panel, is conserved for the superconducting phase transition.

necessary to describe the data. The zero-field superconducting electronic contribution to the specific heat $C_e(T)$ is obtained with $C_e = C(H = 0) - C_n$, as shown in Fig. 3(b). The superconducting transition is a second-order phase transition which requires the entropy conservation. The entropy conservation is evidenced in the inset of Fig. 3(b). The dimensionless specific-heat jump $C_e/\gamma_n T_{sc} \sim 1.0$ at T_{sc} is smaller than the weak coupling value 1.43 described in the BCS theory [32], and is comparable to the value reported in Ref. [8]. To examine the superconducting order parameter of V_2Ga_5, the data above the nuclear Schottky anomaly ($T > 0.2$ K) are fitted to a single-gap s-wave, a line-node with d-wave, and two-gap s-wave models with the following equation

$$C_e = 2N(0)\beta k\frac{1}{4\pi}\int_0^{2\pi} d\phi \int_0^{\pi} d\theta \sin\theta \times \int_{-\hbar\omega_D}^{\hbar\omega_D} -\frac{\partial f}{\partial E}\left(E^2 + \frac{1}{2}\beta\frac{d\Delta^2}{d\beta}\right)d\varepsilon, \tag{4}$$

where $N(0)$ is the density of states at the Fermi surface, $\beta = 1/k_B T$, $E = (\varepsilon^2 + \Delta^2)^{1/2}$, $f = (1 + e^{\beta E})^{-1}$, $\Delta = \Delta_0$ the

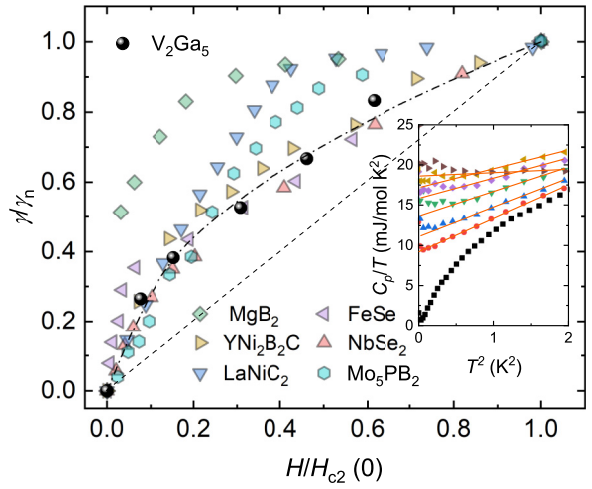

FIG. 4. Normalized specific heat coefficient γ/γ_n vs. normalized magnetic field $H/H_{c2}(0)$ for V_2Ga_5 and other two-gap superconductors. γ is obtained from a linear fit of C/T vs. T^2 and its extrapolation to absolute zero (see inset and text for details). The legends in the inset are identical to the ones of Fig. 3(a). Dashed and dashed-dotted lines represent one-gap theoretical models with isotropic and line nodal gap structures, respectively. The data of reference two-gap superconductors are adopted from Refs. [33–38].

superconducting gap for an isotropic s-wave, $\Delta = \Delta_0 \cos 2\phi$ for line nodes with d-wave symmetry, and $\Delta = \Delta_1 \cdot x + \Delta_2 \cdot (1-x)$ where x is relative weighting for two-gap s-wave. From the fitting result, it is obvious the one-gap s-wave cannot describe the data. For the line-nodal d-wave model, the fit agrees well with the data between T_{sc} and 0.5 K but becomes unsatisfactory at lower temperatures. Finally, an excellent fit using a two-gap s-wave model with $2\Delta_1/k_B T_{sc} = 3.6$ and $2\Delta_2/k_B T_{sc} = 1.5$, with a relative weighting of 55% and 45%, respectively, across the entire fitting range is observed. The two superconducting gap values obtained from this fit are 0.543 and 0.226 meV. Therefore we conclude V_2Ga_5 is a two-gap s-wave superconductor. This conclusion can only be drawn if specific heat measurements are conducted below 0.5 K. Above 0.5 K, both the two-gap s-wave and d-wave models can describe the data equally well [8]. We further studied the vortex excitations in the mixed state by considering the field dependence of the electronic specific heat coefficient $\gamma(H)$. Figure 4 shows $\gamma(H)$ of V_2Ga_5 where the data points were obtained from the linear extrapolations in a C/T vs T^2 plot, as shown in the inset. The fitting of the data was obtained from the relatively high-temperature region to avoid the influence of nuclear contributions from the low-temperature regime. Apparently, $\gamma(H)$ does not follow the linear behavior for an isotropic s-wave model. It is however in line with the power-law behavior $\gamma \sim H^{1/2}$ for nodal superconductor, as shown by the dashed-dotted line. Such a power-law dependence of $\gamma(H)$ has also been observed in other two-gap superconductors YNi_2B_2C [34], $NbSe_2$ [35], and FeSe [37]. At first glance, the nodal model describing $\gamma(H)$ seems incompatible with the two-gap s-wave model that describes C_e/T [see Fig. 3(b)]. However, when the superconducting gap is highly anisotropic, such a discrepancy could be reconciled [34]. In certain extreme cases among two-gap

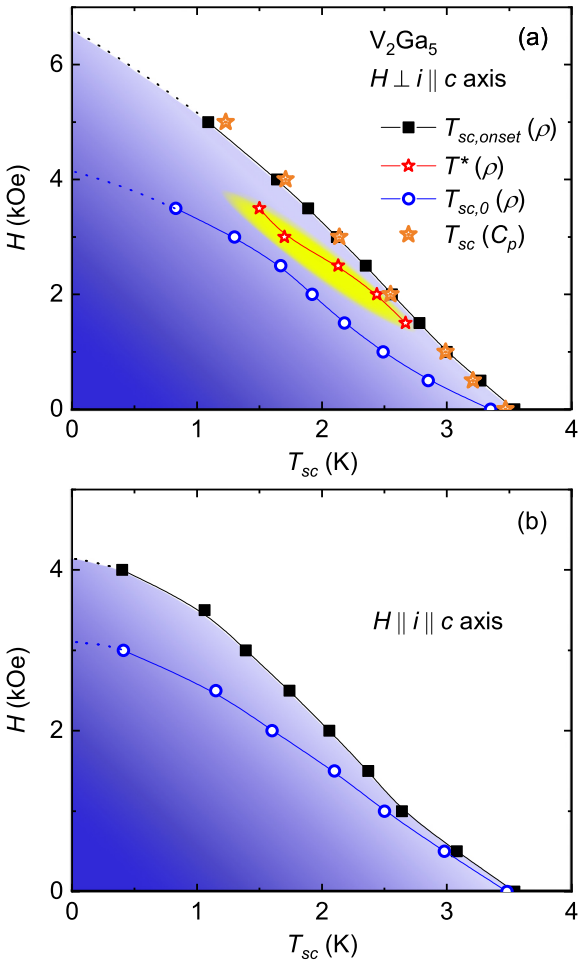

FIG. 5. (a) H-T_{sc} phase diagram with the magnetic field applied perpendicular to the c axis. A yellow oval represents the region of peak effect. T^* denotes the temperature of the resistivity maximum within the superconducting state, i.e., the red arrows in Fig. 2(a). $T_{sc,\mathrm{onset}}$ denotes the temperatures where ρ starts to drop. $T_{sc,0}$ denotes the temperature where ρ becomes zero. T_{sc} is the transition temperature determined from specific heat measurements. (b) H-T_{sc} phase diagram with the magnetic field applied parallel to the c axis. Same legends are applied for (a) and (b).

superconductors, such as MgB_2 [33] and $LaNiC_2$ [36], the smaller superconducting gap is closed at the magnetic field strength much smaller than H_{c2}. This results a rapid increase of γ at low fields and then an gradual saturation with increasing H, as shown in Fig. 4.

We summarize the data from resistivity and specific heat measurements to construct the H-T_{sc} phase diagrams with the magnetic field applied parallel and perpendicular to the c axis, as shown in Fig. 5. The $T_{sc,\mathrm{onset}}$ value determined from $\rho(T)$ coincides with the one determined from $C(T)$.

E. Muon spin relaxation

To further clarify the nature of the superconducting state in V_2Ga_5, we have performed muon spin relaxation (μSR) measurements, as summarized in Fig. 6. Muons are highly sensitive to their local magnetic environment, making them an excellent probe of the vortex state of type II

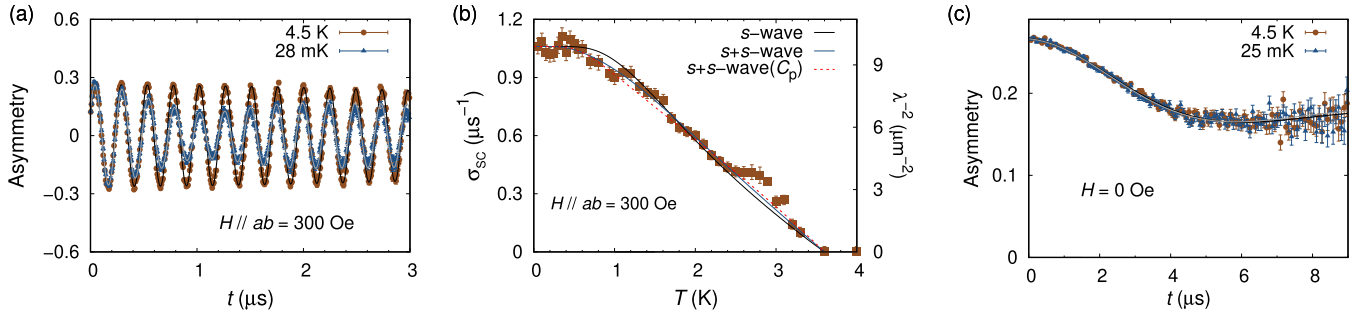

FIG. 6. (a) Representative transverse field μSR spectra for V_2Ga_5 above and below its T_{sc} collected with a magnetic field applied parallel to the *ab*-plane and muon spin parallel to the *c*-direction. The muon precession in the applied field, which gives rise to the oscillatory behavior in the decay asymmetry, shows an increasing relaxation upon entering the vortex state. The fits to the data at 25 mK (grey line) and 4.5 K (black line) are given by Eq. 5 as described in the text. These fits yield (b) the superconducting contribution to the muon Gaussian relaxation rate σ_{SC} as a function of temperature. An improved fit is obtained by fitting the data with two *s*-wave gaps (blue line) as compared to a single *s*-wave gap (black line). The two *s*-wave gap fit is consistent with the results from specific heat, as shown by the dashed red line. (c) Zero-field μSR spectra above and below T_{sc} collected with the muon spin parallel to the *ab* plane show no evidence for time-reversal symmetry breaking. The data are fitted by a Kubo-Toyabe function at 25 mK (grey line) and 4.5 K (black line).

superconductors as well as spontaneous time-reversal symmetry breaking. We begin by investigating the former, where considering the values of $H_{c1,\perp c}$ and $H_{c2,\perp c}$ extracted from our bulk characterization, the sample is expected to be in the vortex state for an applied field of 300 Oe applied $\perp c$ used in our transverse field μSR measurement. In the vortex state, we expect an inhomogenous field distribution due to the presence of a flux line lattice (FLL), which results in a decay of the precession signal as a function of time. The decay in the superconducting state can be clearly seen if we compare the transverse field spectra collected above and below T_{sc}, at 25 mK and 4.5 K as shown in Fig. 6(a).

We fit the transverse field asymmetry spectra with a two term sinusoidal decaying function,

$$G_{\rm TF}(t) = A\left[f\exp\left(\frac{-\sigma^2t^2}{2}\right)\cos(\omega_1 t+\phi) + (1-f)\exp(-\psi t)\cos(\omega_2 t+\phi)\right], \quad (5)$$

where the first term captures the signal coming from fraction, f, of muons stopping inside the sample, while the second term captures the background signal from the fraction, $1-f$ of muons stopping inside the silver sample holder. The precession frequencies of muons in the sample and the background are given by ω_1 and ω_2, respectively, A is the total asymmetry, ϕ is the initial phase of the muons, and σ and ψ are depolarization rates of the sample and the background signals, respectively. The total asymmetry, A, the fraction, f, and the background relaxation rate, ψ, are all expected to be temperature independent and were therefore fitted globally while all other fitted parameters were allowed to vary with temperature. The resulting fits are shown by the solid lines in Fig. 6(a).

The superconducting relaxation rate (σ_{sc}) reflects the mean square inhomogeniety in the field experienced by the muons due to the FLL [39]. This quantity was extracted from the fitted Gaussian relaxation rate σ by subtracting off a smaller, temperature-independent contribution from randomly oriented nuclear dipole moments (σ_N), which give rise to a constant relaxation above T_{sc}. The details of this analysis are described in detail in the Supplemental Material. The resulting temperature dependence of σ_{sc} for V_2Ga_5 at 300 Oe is plotted in Fig. 6(b). The penetration depth can be calculated from the relaxation rate [40], which then allows a direct calculation of the temperature dependence of the superconducting energy gap [41]. The full protocol for performing these calculations is provided in Ref. [10].

In order to further investigate the superconducting gap structure for V_2Ga_5, we have attempted fits of σ_{SC} with both a single *s*-wave gap and two *s*-wave gaps. We note a hump in σ_{SC} between 2.5 and 3.0 K that cannot be explained by either of the gap structures under consideration here. We attribute this feature to the movement of vortices and it is likely also related to the peak effect observed in resistivity measurements below T_{sc}. In our fits, we therefore exclude this range of temperatures. The resulting single *s*-wave gap and two *s*-wave gaps, as shown with solid black and blue lines in Fig. 6(b) with the fitting parameters given in the Supplemental Material. The overall quality of the fit is higher for the two gap function, consistent with heat capacity, particularly in the temperature range close to 1 K. For comparison, we show the calculated temperature dependence of σ_{SC} based on the two gaps extracted from specific heat by a red dashed-line. Considering the level of noise in the data, we consider the gap values extracted from heat capacity to be more reliable.

Finally, we performed zero field μSR measurements to look for any sign of spontaneous magnetic fields and time-reversal symmetry breaking as V_2Ga_5 enters its superconducting state. The magnetic field at the sample position was carefully zeroed following the protocol described in the methods. High statistics zero field spectra were collected above and below T_{sc} with representative spectra shown in Fig. 6(c). In the absence of any static electronic moments, the muon polarization decay is due to randomly oriented nuclear magnetic moments, as described by the Gaussian Kubo-Toyabe function,

$$G_{\rm KT}(t) = \tfrac{1}{3} + \tfrac{2}{3}(1-\sigma^2t^2)e^{-\frac{\sigma^2t^2}{2}}, \quad (6)$$

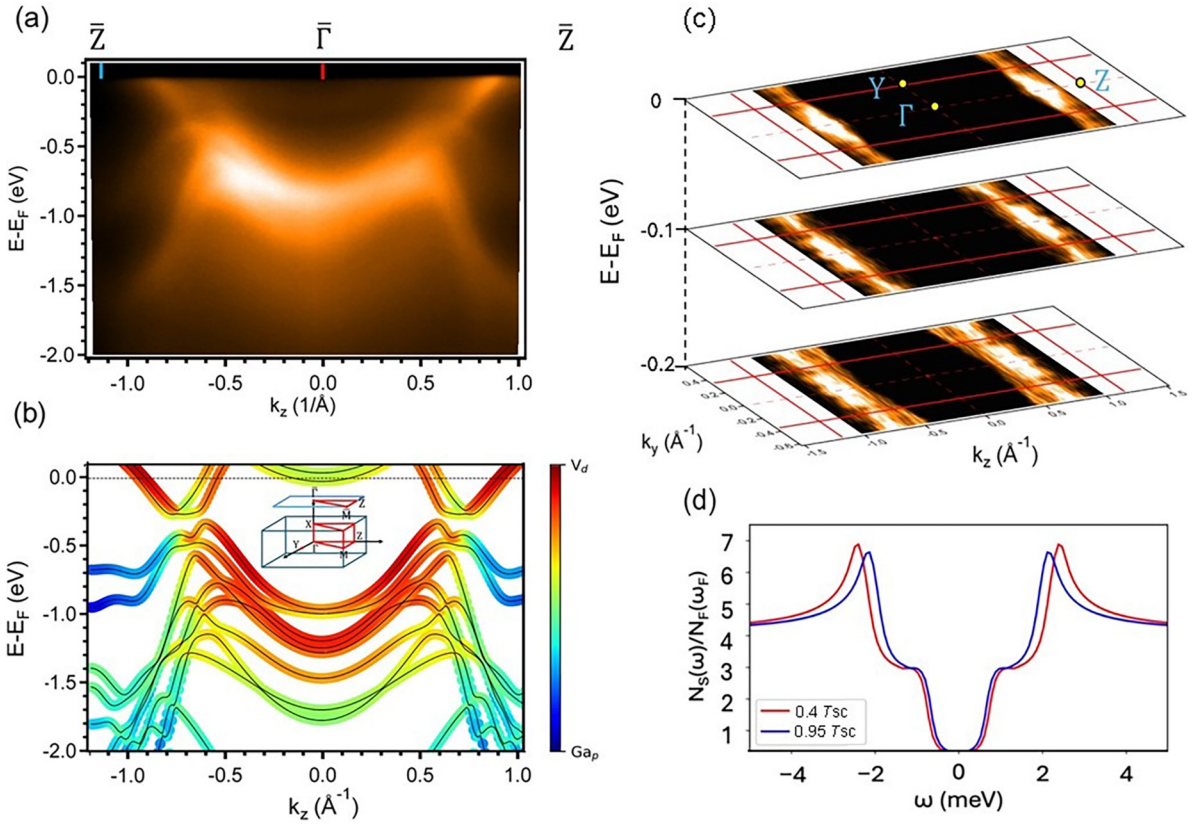

FIG. 7. (a) ARPES spectrum of V_2Ga_5 were acquired along the k_z direction at 89 K using a photon energy of 78 eV. (b) Calculated band dispersion of V_2Ga_5 along k_z direction at $(k_x, k_y) = (0.133\,\text{Å}^{-1}, 0)$. The amount of the projected orbital weight of V *d* orbital and Ga *p* orbital is represented by red and blue curves, respectively. The color bar indicates the corresponding mixed contribution. (c) Constant energy contours of V_2Ga_5 at distinct binding energies with respect to the Fermi surface: 0, 0.1, and 0.2 eV, which were measured at 89 K with 78 eV photon energy. (d) Quasiparticle density of states for V_2Ga_5 in the superconducting state at different temperatures ($0.4T_{sc}$ and $0.95T_{sc}$).

where σ reflects the width of the field experienced by muons due to nuclear dipoles. The total fitting function applied to our zero field data is

$$A(t) = A[fG_{\text{KT}}(t)e^{-\Lambda t} + (1 - f)], \tag{7}$$

where A is the sample asymmetry, f represents the asymmetry fraction originating from muons that land in the sample, and Λ, represents any additional relaxation inside the sample, such as that coming from spontaneous fields inside the superconducting state. The zero field muon spin relaxation rate for V_2Ga_5 is mainly attributed to a temperature-independent contribution from nuclear dipole moments. No statistically significant change in Λ is observed at temperatures well below T_{sc}, as can be evidenced from the comparison of spectra collected at 25 mK and 4.5 K shown in Fig. 6(c). We conclude from our data that no significant breaking of time-reversal symmetry occurs in the superconducting state. Considering the lack of evidence for TRS breaking and the gap being well fitted with two *s*-wave gaps, we conclude that the superconductivity in V_2Ga_5 arises from a singlet pairing.

F. Angle-resolved photoemission spectroscopy and band-structure calculations

To elucidate the nature of superconductivity in V_2Ga_5, we conducted ARPES experiments and performed the density functional theory (DFT) calculations to unveil the band structure of V_2Ga_5. Figure 7(a) illustrates the band mapping result of ARPES spectra along the Γ-Z direction, measured at 89 K utilizing a photon energy of 78 eV. Two discernible bands across the Fermi level were observed: one electron band below −0.25 eV of binding energy around the Z point disperses toward the Fermi level, while another, with weaker photoemission intensity, behaves as a parabolic band around the Γ point. To gain insight into the out-of-plane band dispersion, we employed a photon energy-dependent ARPES experiment [42], using energies ranging from 52 to 86 eV. No significant changes are observed in bands around the Fermi level, suggesting only weakly dispersive behavior along the k_x direction, which is revealed in Ref. [10]. The needlelike V_2Ga_5 single crystal exhibits a fourfold symmetry in the *a*-*b* plane with a much longer lattice constant compared with the *c* axis, resulting in a quasi one-dimensional behavior of the band structure. The highly dispersive band structure with periodic behavior shown in Fig. 7 corresponds to the periodicity of reciprocal space of the *c* axis. Additionally, constant energy mapping in Fig. 7(c) demonstrates a less dispersive behavior for these bands around the Fermi level along the k_y direction, without the presence of nodes on the Fermi surface [10].

Figure 7(b) presents the calculated band structure of V_2Ga_5 along the Γ-Z direction at $(k_x, k_y) = (0.133\,\text{Å}^{-1}, 0)$, where the orbital contribution for each energy eigenstate is analyzed

and the projected weight of V d orbital and Ga p orbital is represented by red and blue curves, respectively. The measured bands in the low binding energy region are mainly composed of the V $3d$ and Ga $4p$ orbitals, and the calculated band structure at $k_x = 0.133\,\text{Å}^{-1}$ aligns well with the ARPES spectra. As presented in Ref. [10], these bands show less dispersion along the k_x direction, suggesting a quasi-one-dimensional behavior.

Through first-principles calculations, we have identified three bands that cross the Fermi level, and all of them are responsible for the observed two-gap superconductivity. Using the linear response framework (see Ref. [10]), the electron-phonon coupling strength (λ) has been calculated. The result yields a theoretical electron-phonon coupling strength of 0.75 and a superconducting critical temperature (T_{sc}) of 7.38 K based on the McMillan-Allen-Dynes formula [43,44]:

$$T_{sc} = \frac{\omega_{\log}}{1.2} \exp\left[\frac{-1.04(1+\lambda)}{\lambda - \mu_c^*(1+0.62\lambda)}\right]. \tag{8}$$

Here, the typical Coulomb pseudopotential value μ_c^* is set to 0.1. We have further solved the anisotropic Migdal-Eliashberg equations to investigate the temperature dependence of the superconducting gap. In Fig. 7(d), the quasiparticle density of states in the superconducting state is presented at $0.4T_{sc}$ and $0.95T_{sc}$. It clearly shows the two-gap behavior, similar to that in the two-gap superconductor MgB_2. The calculated T_{sc} and the nodeless Fermi surface are in agreement with our experimental observations, and our theoretical result of the two-gap s-wave behavior is also consistent with the recent experimental findings [8]. However, we note that the theoretical two-gap values are overestimated compared to the experimental ones. This discrepancy requires further theoretical work to reconcile, such as first-principles calculations of the Coulomb pseudopotential.

IV. SUMMARY

We present a detailed study of the physical properties and electronic structure of the superconductor V_2Ga_5. From resistivity measurements with the magnetic field applied parallel and perpendicular to the c axis, the H_{c2} versus T phase diagrams are constructed, where small magnetic anisotropy has been registered. Resistivity under high pressure shows that the superconductivity is suppressed linearly with pressure, suggesting the superconductivity is phonon-mediated. Low-temperature specific heat and μSR experiments both reveal that the two-gap s-wave model best describes the superconducting order parameter. These two gaps can be directly inferred from ARPES measurements and are further supported by band structure calculations. By combining various experiments with theoretical calculations, our findings intricately detail the physical properties and superconductivity of V_2Ga_5, paving the way for future studies. For example, it would be interesting to investigate the in-plane magnetic anisotropy when the magnetic field is applied perpendicular to the c axis, which we were unable to perform due to the limitations of the crystal morphology.

ACKNOWLEDGMENTS

We thank R. Pierre and T. Klein for fruitful discussions. We thank Dr. M.-K. Lee and C.-C. Yang at PPMS-16T and SQUID VSM Labs, Instrumentation Center, National Cheng Kung University (NCKU) for technical support. We are grateful to P.-Z. Hsu and L.-J. Chang for the help of Laue diffraction. C.-L.H. would like to thank Academia Sinica for "Short-term Domestic Visiting Scholars" program in the Nanomaterial and Low Temperature Physics Laboratory, IOP, Academia Sinica. This work is supported by National Science and Technology Council in Taiwan (Grant No. NSTC 109-2112-M-006-026-MY3, NSTC 110-2124-M-006-011, and NSTC 112-2112-M-032-010) and the Higher Education Sprout Project, Ministry of Education to the Headquarters of University Advancement at NCKU. W.-T.C. acknowledges the National Science and Technology Council in Taiwan, for funding 111-2112-M-002-044-MY3, 112-2124-M-002-012, Academia Sinica Project No. AS-iMATE-111-12, and the Featured Areas Research Center Program within the framework of the Higher Education Sprout Project by the Ministry of Education of Taiwan 113L9008. L.Z.D. would like to thank U.S. Air Force Office of Scientific Research Grants No. FA9550-15-1-0236 and No. FA9550-20-1-0068; the T. L. L. Temple Foundation; the John J and Rebecca Moores Endowment; the State of Texas through the Texas Center for Superconductivity at the University of Houston. A.M.H. acknowledges support from the Natural Sciences and Engineering Research Council of Canada (NSERC), the CIFAR Azrieli Global Scholars program, and the Sloan Research Fellowships program. Research at UBC was undertaken, in part, thanks to funding from the Canada First Research Excellence Fund, Quantum Materials and Future Technologies Program. C.-C.L. acknowledges support from the National Center for Theoretical Sciences (NCTS) of Taiwan.

[1] P. C. Canfield and Z. Fisk, Growth of single crystals from metallic fluxes, Philosophical Magazine B **65**, 1117 (1992).

[2] M. G. Kanatzidis, R. Pöttgen, and W. Jeitschko, The metal flux: A preparative tool for the exploration of intermetallic compounds, Angew. Chem., Int. Ed. **44**, 6996 (2005).

[3] B. B. Goodman, The thermodynamic properties of superconducting V_3Ga, Phys. Lett. **1**, 215 (1962).

[4] A. Junod, J.-L. Staudenmann, J. Muller, and P. Spitzli, Superconductivity, density-of-states models, and specific heat of A15-type compounds V-Ga and V-Si, J. Low Temp. Phys. **5**, 25 (1971).

[5] E. Cruceanu, G. Antesberger, and C. Papastaikoudis, Low-temperature electrical properties of V_2Ga_5, Solid State Commun. **15**, 1047 (1974).

[6] K. C. Lobring, C. E. Check, J. Zhang, S. Li, C. Zheng, and K. Rogacki, Single crystal growth, bonding analysis and superconductivity of V_2Ga_5, J. Alloys Compd. **347**, 72 (2002).

[7] A. Teruya, M. Takeda, A. Nakamura, H. Harima, Y. Haga, K. Uchima, M. Hedo, T. Nakama, and Y. Ōnuki, Characteristic

fermi surface properties of V_2Ga_5, $CoGa_3$, $TiGa_3$, $ZrGa_3$, and $ZrAl_3$ with different tetragonal structures, J. Phys. Soc. Jpn. **84**, 054703 (2015).

[8] C. Q. Xu, C. C. Zhao, Y. Shen, D. Ratkovski, X. Ma, W. Zhou, X. Yin, B. Li, A. F. Bangura, C. Cao, B. Wang, Z. Zhu, X. Ke, D. Qian, S. Li, and X. Xu, Multigap nodeless superconductivity in the dirac intermetallic alloy V_2Ga_5 with one-dimensional vanadium chains, Phys. Rev. B **109**, L100506 (2024).

[9] A. A. Coelho, Topas and topas-academic: an optimization program integrating computer algebra and crystallographic objects written in C++, J. Appl. Crystallogr. **51**, 210 (2018).

[10] See Supplemental Material at http://link.aps.org/supplemental/10.1103/PhysRevResearch.6.033253 for details of k_x dependence of band structure.

[11] G. D. Morris and R. H. Heffner, A method of achieving accurate zero-field conditions using muonium, Phys. B: Condens. Matter **326**, 252 (2003).

[12] A. Suter and B. M. Wojek, Musrfit: a free platform-independent framework for μSR data analysis, Phys. Procedia **30**, 69 (2012).

[13] P. Giannozzi, O. Andreussi, T. Brumme, O. Bunau, M. B. Nardelli, M. Calandra, R. Car, C. Cavazzoni, D. Ceresoli, M. Cococcioni, N. Colonna, I. Carnimeo, A. D. Corso, S. de Gironcoli, P. Delugas, R. A. DiStasio, A. Ferretti, A. Floris, G. Fratesi, G. Fugallo *et al.*, Advanced capabilities for materials modelling with quantum espresso, J. Phys.: Condens. Matter **29**, 465901 (2017).

[14] S. Poncé, E.R. Margine, C. Verdi, and F. Giustino, Epw: Electron–phonon coupling, transport and superconducting properties using maximally localized wannier functions, Comput. Phys. Commun. **209**, 116 (2016).

[15] J. H. N. van Vucht, H. A. C. M. Bruning, H. C. Donkersloot, and A. H. Gomes de Mesquita, The system vanadium-gallium, Philips Res. Repts. **19**, 407 (1964).

[16] B. D. Cullity and C. D. Graham, *Introduction to Magnetic Materials* (John Wiley & Sons, NY, 2008), Chap. 16, pp. 517–526.

[17] C. Kittel, *Introduction to solid state physics* (John Wiley & Sons, NY, 2004).

[18] C. V. Tomy, G. Balakrishnan, and D. McK. Paul, Observation of the peak effect in the superconductor $Ca_3Rh_4Sn_{13}$, Phys. Rev. B **56**, 8346 (1997).

[19] S. H. Autler, E. S. Rosenblum, and K. H. Gooen, High-field superconductivity in niobium, Phys. Rev. Lett. **9**, 489 (1962).

[20] M. J. Higgins and S. Bhattacharya, Varieties of dynamics in a disordered flux-line lattice, Physica C: Superconductivity and its Applications **257**, 232 (1996).

[21] M. Hedo, Y. Kobayashi, Y. Inada, E. Yamamoto, Y. Haga, J.-ichi Suzuki, N. Metoki, Y. Ōnuki, H. Sugawara, H. Sato, K. Tenya, T. Tayama, H. Amitsuka, and T. Sakakibara, Peak effect in $CeRu_2$: Role of crystalline defects, J. Phys. Soc. Jpn. **67**, 3561 (1998).

[22] S. Chaudhary, A. K. Rajarajan, K. J. Singh, S. B. Roy, and P. Chaddah, Peak effect in the vortex state of V_3Si: a study of history dependence, Physica C: Superconductivity **353**, 29 (2001).

[23] H.-S. Lee, D.-J. Jang, B. Kang, H.-G. Lee, I. J. Lee, Y. Jo, M.-H. Jung, M.-H. Cho, and S.-I. Lee, Relationship between surface superconductivity, bulk superconductivity and the peak effect in MgB_2 single crystals, New J. Phys. **10**, 063003 (2008).

[24] U. S. Kaluarachchi, Q. Lin, W. Xie, V. Taufour, S. L. Bud'ko, G. J. Miller, and P. C. Canfield, Superconducting properties of $Rh_9In_4S_4$ single crystals, Phys. Rev. B **93**, 094524 (2016).

[25] R. Willa, A. E. Koshelev, I. A. Sadovskyy, and A. Glatz, Peak effect due to competing vortex ground states in superconductors with large inclusions, Phys. Rev. B **98**, 054517 (2018).

[26] B. Lorenz and C. W. Chu, *High Pressure Effects on Superconductivity*, Frontiers in Superconducting Materials (Springer, Berlin, Heidelberg, 2005).

[27] D. H. Chung and W. R. Buessem, The Voigt-Reuss-Hill approximation and elastic moduli of polycrystalline MgO, CaF_2, β-ZnS, ZnSe, and CdTe, J. Appl. Phys. **38**, 2535 (1967).

[28] C.-S. Man and M. Huang, A simple explicit formula for the Voigt-Reuss-Hill average of elastic polycrystals with arbitrary crystal and texture symmetries, J. Elast. **105**, 29 (2011).

[29] K. Grube (private communication).

[30] G. H. Fuller, Nuclear Spins and Moments, J. Phys. Chem. Ref. Data **5**, 835 (1976).

[31] A. Steppke, M. Brando, N. Oeschler, C. Krellner, C. Geibel, and F. Steglich, Nuclear contribution to the specific heat of $Yb(Rh_{0.93}Co_{0.07})_2Si_2$, Physica Status Solidi (b) **247**, 737 (2010).

[32] J. Bardeen, L. N. Cooper, and J. R. Schrieffer, Theory of superconductivity, Phys. Rev. **108**, 1175 (1957).

[33] F. Bouquet, R. A. Fisher, N. E. Phillips, D. G. Hinks, and J. D. Jorgensen, Specific heat of $Mg^{11}B_2$: Evidence for a second energy gap, Phys. Rev. Lett. **87**, 047001 (2001).

[34] C. L. Huang, J.-Y. Lin, C. P. Sun, T. K. Lee, J. D. Kim, E. M. Choi, S. I. Lee, and H. D. Yang, Comparative analysis of specific heat of YNi_2B_2C using nodal and two-gap models, Phys. Rev. B **73**, 012502 (2006).

[35] C. L. Huang, J.-Y. Lin, Y. T. Chang, C. P. Sun, H. Y. Shen, C. C. Chou, H. Berger, T. K. Lee, and H. D. Yang, Experimental evidence for a two-gap structure of superconducting $NbSe_2$: A specific-heat study in external magnetic fields, Phys. Rev. B **76**, 212504 (2007).

[36] J. Chen, L. Jiao, J. L. Zhang, Y. Chen, L. Yang, M. Nicklas, F. Steglich, and H. Q. Yuan, Evidence for two-gap superconductivity in the non-centrosymmetric compound $LaNiC_2$, New J. Phys. **15**, 053005 (2013).

[37] J. T. Chen, Y. Sun, T. Yamada, S. Pyon, and T. Tamegai, Two-gap features revealed by specific heat measurements in FeSe, J. Phys.: Conf. Ser. **871**, 012016 (2017).

[38] T. Shang, W. Xie, D. J. Gawryluk, R. Khasanov, J. Z. Zhao, M. Medarde, M. Shi, H. Q. Yuan, E. Pomjakushina, and T. Shiroka, Multigap superconductivity in the Mo_5PB_2 boron–phosphorus compound, New J. Phys. **22**, 093016 (2020).

[39] E. H. Brandt, Magnetic field density of perfect and imperfect flux line lattices in type II superconductors. I. application of periodic solutions, J. Low Temp. Phys. **73**, 355 (1988).

[40] E. H. Brandt, Properties of the ideal ginzburg-landau vortex lattice, Phys. Rev. B **68**, 054506 (2003).

[41] A. Carrington and F. Manzano, Magnetic penetration depth of MgB_2, Physica C: Superconductivity **385**, 205 (2003).

[42] A. Damascelli, Probing the electronic structure of complex systems by arpes, Phys. Scr. **T109**, 61 (2004).

[43] W. L. McMillan, Transition temperature of strong-coupled superconductors, Phys. Rev. **167**, 331 (1968).

[44] P. B. Allen and R. C. Dynes, Transition temperature of strong-coupled superconductors reanalyzed, Phys. Rev. B **12**, 905 (1975).